# We are IntechOpen,
# the world's leading publisher of
# Open Access books
# Built by scientists, for scientists

## 6,900
Open access books available

## 185,000
International authors and editors

## 200M
Downloads

## 154
Countries delivered to

Our authors are among the

## TOP 1%
most cited scientists

## 12.2%
Contributors from top 500 universities

CLARIVATE ANALYTICS
**BOOK CITATION INDEX**
INDEXED

**WEB OF SCIENCE**™

Selection of our books indexed in the Book Citation Index
in Web of Science™ Core Collection (BKCI)

## Interested in publishing with us?
## Contact book.department@intechopen.com

# Array Pattern Synthesis for ETC Applications

*Daniele Inserra and Guangjun Wen*

## Abstract

The problem of antenna array synthesis for radiation pattern defined on a planar surface will be considered in this chapter. This situation could happen when the electric field $r$-decay factor effect cannot be neglected, for example, an antenna array mechanically tilted and a pattern defined in terms of Cartesian coordinates, as in the electronic toll collection (ETC) scenario. Two possible approaches will be presented: the first one aims at the precise synthesis of the pattern in the case both a constant power-bounded area and a sidelobe suppression region are defined and required to be synthesized. The second approach instead devotes at stretching the coverage area toward the travel length (without considering a precise definition of the communication area) to increase the available identification time with an iterative methodology. For the latter, an antenna prototype has been fabricated, and measurement results have confirmed the approach validity.

**Keywords:** antenna arrays, radiation pattern synthesis, linear programming, electronic toll collection (ETC), radio frequency identification (RFID)

## 1. Introduction

Most parts of literature on antenna array describe the synthesis of the *array factor* [1]. In fact, when the antenna array elements are the same, and assuming that the single antenna beamwidth is broader than that of the final array, it is possible to observe that the magnitude of the array factor is proportional to that of the total radiated electric field. Lots of synthesis methodologies have been presented over the years for both simple array structures, for example, linear uniform arrays [2], and more complex geometries (which require the use of optimization algorithms) [3–7]. Nevertheless, there exist other situations which require the whole electric field behavior control and, in particular, its $r$-decay behavior. In literature, these problems are called *beam-shaped pattern* or *contoured pattern synthesis*. Possible applications for these methods are in the field of satellite communications where small antennas or antenna arrays are employed for illuminating a profiled reflector, as described in [8]. Besides the use of a profiled reflector, other techniques have been developed and proposed [9–12]. The minimum least square error (MLSE) criteria are used in [9] for the synthesis of a desired contoured pattern specified with points in the angular domain. Moreover, a discrete Fourier transform (DFT) shape of the synthesis function is assigned to provide a better radiation control. In [10], a successive projection

method (SPM) procedure is developed which exploits a new set of basis functions instead of the DFT. This reduces the number of optimization variables with respect to the conventional SPM [11]. Another example of synthesis technique which minimizes the difference with a desired pattern in an iterative fashion can be found in [12].

Besides the case of satellite communications, there exist other applications in the context of vehicular communications and, in particular, for vehicle-to-infrastructure connection and vice versa, in which the electric field $r$-decay behavior affects the beam pattern, for example, a road side unit (RSU) equipped with an antenna array which has to radiate toward a specific area, defined on the road surface, for dedicated short-range communications (DSRC). This specific problem is usually not addressed as a beam-shaped pattern problem because nowadays electronic toll collection (ETC) is still performed with low-speed dedicated corridor sufficient to guarantee the automatic vehicle identification (AVI). However, in the futuristic envision of multilane free flow (MLFF) in which vehicles will perform tolling operation without reducing travel speed [13], an efficient beam pattern synthesis will become fundamental. In order to better highlight this point, let us consider **Figure 1**, in which a MLFF situation is depicted. In this example, each roadlane is managed by a dedicated RSU antenna array which radiates a certain beam pattern on the road surface.

If this beam pattern is synthesized for guaranteeing the correct communication between RSU and on-board unit (OBU) within a certain coverage area of length $l_{ca}$, it is possible to approximate the maximum available time to perform the toll transaction $\tau_{trav}$ as a function of the vehicle speed $v_{car}$, as shown in **Figure 2** [14]. Obviously, the vehicle speed increase reduces the available transaction time, making the ETC system design more challenging. Nonetheless, the length of the coverage area $l_{ca}$ is also fundamental to increase the available transaction time and relax the ETC system requirements, and for this reason, the antenna array beam pattern synthesis should be carefully optimized.

Motivated by the above considerations, the problem of antenna array synthesis when the electric field $r$-decay effect cannot be neglected is treated in this chapter, with particular emphasis on the context of vehicular communications where a RSU equipped with a mechanically tilted antenna array has to radiate a beam pattern defined on the road surface. The problem will be addressed in two different ways: firstly, a generic optimization problem will be presented for the case of a precise pattern definition; a circular objective area will be considered and synthesized together with a suppression surrounding area (useful for guaranteeing a minimum sidelobe level margin) [15]; and then, the coverage area stretching toward the travel
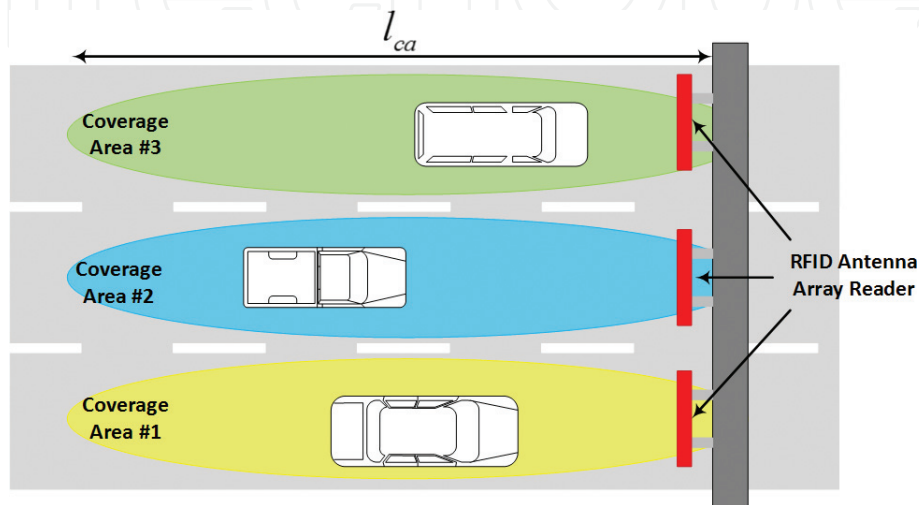


**Figure 1.**
*Example of three-roadway highway tolling system with RFID antenna reader.*
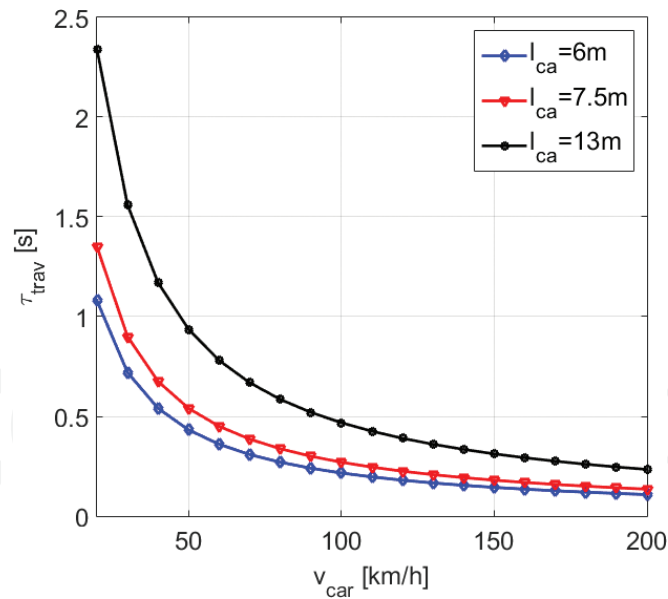
**Figure 2.**
*Maximum available transaction time as function of the vehicle speed.*

direction will be investigated with the objective of increasing the available transaction time for radio frequency identification (RFID)-based DSRC, and a simple iterative approach will be presented [16]. Both the presented methodologies will be analyzed with the aid of numerical results. Moreover, the second approach will be confirmed by experimental results.

## 2. Problem statement and reference system description

Let us consider the design of an antenna array. The total electric field radiated by an array of identical antenna elements can be written by using the well-known pattern multiplication property [2] and reads

$$\overline{E}_{tot}(r, \phi, \theta) = \overline{E}_0(r, \phi, \theta) \cdot AF(\phi, \theta) \qquad (1)$$

where $\overline{E}_0(r, \phi, \theta)$ is the single antenna electric field vector and $AF(\phi, \theta)$ is the array factor. By assuming that the single antenna beamwidth is broader than the desired one, only the term $AF(\phi, \theta)$ can be considered in the design. Nonetheless, the single antenna radiation pattern can also be included in the synthesis process. In fact, if $\overline{E}_0(r, \phi, \theta)$ can be decomposed as

$$\overline{E}_0(r, \phi, \theta) = \frac{e^{-jk_0 r}}{r} \left( E_\phi \cdot \hat{\phi} + E_\theta \cdot \hat{\theta} \right) \qquad (2)$$

where $k_0$ is the wavenumber, and if the maximum absolute value of the electric field components is $E_0$, then it is possible to define the function:

$$f(\phi, \theta) = \sqrt{\left( \frac{E_\phi}{E_0} \right)^2 + \left( \frac{E_\theta}{E_0} \right)^2} \qquad (3)$$

and to include it into the synthesis process, that is, the function that has to be synthesized becomes $f(\phi, \theta) \cdot AR(\phi, \theta)$. The function $f(\phi, \theta)$ is usually called *antenna pattern*.

It is now clear that the distance $r$ is not included in the synthesis process. For this reason, the synthesized pattern preserves its characteristics uniquely on an $r$-constant surface, that is, a spherical surface. If an arbitrarily beam-shaped pattern is required to be synthesized (a pattern defined on a nonspherical surface), the $r$-decay factor of $\overline{E}_0(r, \phi, \theta)$ must be included into the synthesis process. For this reason, the normalized function that has to be optimized becomes

$$F(\phi, \theta) = \frac{r_0}{r} \frac{f(\phi, \theta)}{f(\phi_0, \theta_0)} \cdot AF(\phi, \theta) \qquad (4)$$

where $(\phi_0, \theta_0)$ is the electrical steering direction and $r_0$ is the reference distance from the antenna array to the synthesis surface (included for function normalization).

Let us assume a RSU with an antenna array placed at height $h_A$ which can be mechanically tilted by an angle $\theta_A$ (this can be required to better address a specific coverage area requirement on a planar surface). In this case, both the array electrical steering direction $(\phi_0, \theta_0)$ and the mechanical tilt steer the beam pattern. **Figure 3(a)** describes this scenario. The coverage area (herein defined as the region where the normalized total electric field on the road surface is larger than a certain threshold value) could be arbitrarily assigned in shape, even if circular or elliptical is a more realistic hypothesis. A coverage area might be required for high-power reception within a high data-rate service spatial area or to guarantee signal reception as it will be described later for the specific case of RFID-based ETC. Furthermore, the synthesized beam sidelobe-level control might also be important to avoid signal interference with other coverage zones illuminated by other RSUs as in **Figure 3(b)**. Finally, other situations could require to limit the coverage area extension toward a specific direction in order to avoid possible overlap with other coverage areas.

**Figure 4** depicts the antenna array reference system in spherical coordinates $r$, $\phi$, and $\theta$ and in Cartesian coordinates $x$, $y$, and $z$ and the coverage area reference system in Cartesian coordinates $x_R$, $y_R$, and $z_R$. Moreover, a RSU is placed on a $h_A$ height pole (or a highway gate tolling station), and the coverage area is defined on the road plane, that is, $z_R = 0$. However, the presented methodology can also address the case in which $z_R = h_{tag}$. It is worth noting that $h_{tag}$ which represents the OBU height (usually installed on the vehicle windshield) depends on the vehicle model and a univocal solution for the coverage area at a fixed height cannot be specified. For this reason, a reference OBU height can be defined for carrying out the synthesis process of the antenna array, and then synthesis results at different heights $h_{tag}$ should be verified.
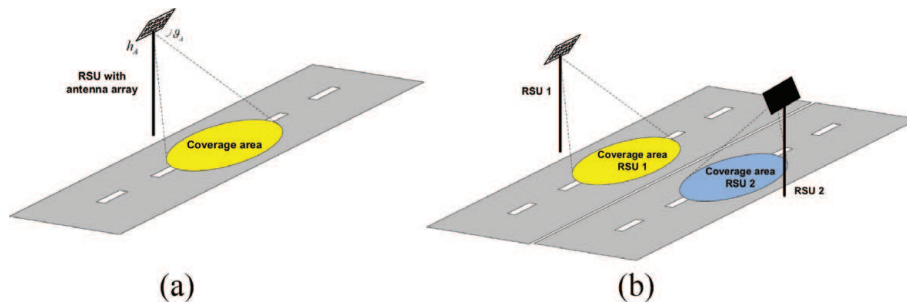


**Figure 3.**
*Example of RSU displacement and coverage areas. (a) RSU with a coverage area defined on a road surface and (b) RSUs with close coverage areas.*
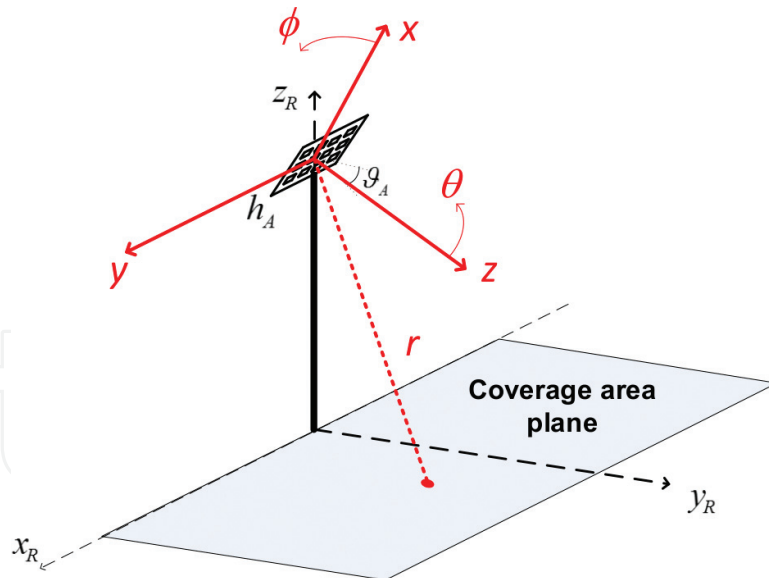
**Figure 4.**
*Antenna array and coverage area reference systems.*

The antenna array reference system can be obtained by a rototranslation of the coverage area reference system [17]. Particularly, the following relations can be obtained:

$$
\begin{cases}
\begin{cases}
x_R = y \\
y_R = \cos(\theta_A)z - \sin(\theta_A)x \\
z_R = \sin(\theta_A)z + \cos(\theta_A)x + h_A
\end{cases} \\
\begin{cases}
x = \sin(\theta_A)y_R + \cos(\theta_A)(z_R - h_A) \\
y = x_R \\
z = \cos(\theta_A)y_R - \sin(\theta_A)(z_R - h_A)
\end{cases} \\
r = \sqrt{x_R^2 + y_R^2 + (z_R - h_A)^2} \\
\phi = \arctan\left\{ \dfrac{x_R}{\sin(\theta_A)y_R + \cos(\theta_A)(z_R - h_A)} \right\} \\
\theta = \arccos\left\{ \dfrac{\cos(\theta_A)y_R - \sin(\theta_A)(z_R - h_A)}{\sqrt{x_R^2 + y_R^2 + (z_R - h_A)^2}} \right\}
\end{cases}
\tag{5}
$$

It should be noted that other synthesis surfaces could be considered with the method herein presented. For the sake of comprehension simplification, and also because it represents a practical situation, the case $z_R$ constant is herein described. In this case, it is straightforward to understand that $r = r(\phi, \theta)$, and then also the normalized function $F(r, \phi, \theta)$ in (4) becomes $F = F(\phi, \theta)$.

## 3. Optimization problem and antenna array synthesis

A generic planar array of $N$ elements lying on the $xy$-plane of **Figure 4** is assumed. The synthesis function in (4) can be written as follows:

$$F(\phi, \theta) = \frac{r_0}{r} \frac{f(\phi, \theta)}{f(\phi_0, \theta_0)} \sum_{n=1}^{N} w_n e^{j(k_x x_n + k_y y_n)} \tag{6}$$

where $k_x = \frac{2\pi}{\lambda_0} \cos(\phi) \sin(\theta)$, $k_y = \frac{2\pi}{\lambda_0} \sin(\phi) \sin(\theta)$, $w_n$ is the $n$th element amplitude excitation, $w_n \in \mathbb{C}$, $n \in \{1, .., N\}$ [18], and $(x_n, y_n)$ is the position of the $n$th antenna element on the $xy$-plane. Let us now consider the case of a synthesis on the plane $z_R = 0$ as illustrated in **Figure 4**. Defining a suppression region $\Sigma$, where the maximum sidelobe level $t = \max_{(\phi_i, \theta_i) \in \Sigma} |F(\phi_i, \theta_i)|$ has to be minimized, that is,

$$|F(\phi_i, \theta_i)| \leq t, (\phi_i, \theta_i) \in \Sigma \tag{7}$$

and a coverage area $C$, where it is desired that the normalized electric field is larger than a certain bound value $P_{bound}$ (expressed in dB), that is,

$$|F(\phi_k, \theta_k)| \geq 10^{P_{bound}/20}, (\phi_k, \theta_k) \in C \tag{8}$$

it is possible to derive the generic optimization problem as

$$
\begin{aligned}
&\min_{\phi_0, \theta_0, w_n, n \in \{1,...,N\}} && t \\
&\text{s.t.} && F(\phi_0, \theta_0) = 1 \\
& && |F(\phi_i, \theta_i)| \leq t, (\phi_i, \theta_i) \in \Sigma \\
& && \left|F(\phi_j, \theta_j)\right| = 10^{P_{\text{bound}}/20}, \left(\phi_j, \theta_j\right) \in B \\
& && |F(\phi_h, \theta_h)| \leq 10^{P_{\text{bound}}/20}, (\phi_h, \theta_h) \in \Omega \\
& && |F(\phi_k, \theta_k)| \leq 1, (\phi_k, \theta_k) \in C \\
& && |F(\phi_k, \theta_k)| \geq 10^{P_{\text{bound}}/20}, (\phi_k, \theta_k) \in C
\end{aligned} \tag{9}
$$

Some additional constraints are included to better define the function trend within the area of interest. In particular, the constraint $\left|F(\phi_j, \theta_j)\right| = 10^{P_{\text{bound}}/20}, \left(\phi_j, \theta_j\right) \in B$ fixes the function value on the coverage area bound $B$, while $|F(\phi_h, \theta_h)| \leq 10^{P_{\text{bound}}/20}, (\phi_h, \theta_h) \in \Omega$ defines a criterion within $\Omega$ that is the space between the coverage area and the suppression region. It is worth noting that $(\phi_i, \theta_i)$ are related to the coordinates $x_R$ and $y_R$ according to (5).

The mechanical tilt $\theta_A$ has not been included in the optimization problem because its choice is usually not arbitrary. It could be preliminarily selected to radiate toward a specific direction, and its choice is left to common sense.

## 3.1 Derivation of suboptimal problem

The steering direction $(\phi_0, \theta_0)$ and the last inequality in (9) lead to a nonlinear optimization problem with a non-convex constraint, and according to [5], the global optimality cannot be guaranteed, with computation time extremely large.

Two hypotheses have been considered for reducing the problem complexity. In particular, a known steering direction $(\phi_0, \theta_0)$ and symmetric antenna array with respect to the axes origin are assumed. Since there is no way to know a priori the optimum steering direction, the first hypothesis will lead to a suboptimal solution based on a common sense selection of the steering direction. Furthermore, it has been observed experimentally that if the array pattern is steered toward the center

point of the coverage area, this always leads to a feasible solution with an acceptable array size. Another criterion for the steering direction choice is to select $(\phi_0, \theta_0)$ in order to synthesize the array factor as much symmetrical as possible [15].

The second hypothesis, instead, addresses the most part of practical cases.

Based on the choice of the steering direction $(\phi_0, \theta_0)$, two main practical cases can be distinguished: the broadside array $(\phi_0 = 0, \theta_0 = 0)$ and the steered array $(\phi_0 \neq 0, \theta_0 \neq 0)$.

### 3.1.1 Broadside array

The broadside array is the most considered case for practical usage. Under the hypothesis of symmetric antenna array with respect to the axes origin, the synthesis function in (4) can be written as follows:

$$F(\phi, \theta) = 2 \frac{r_0}{r} \frac{f(\phi, \theta)}{f(\phi_0, \theta_0)} \sum_{n=1}^{N/2} w_n \cos(k_x x_n + k_y y_n) \tag{10}$$

In this case, the amplitude excitations $w_n \in \mathbb{R}$, $n \in \{1, .., N\}$ [18], and, consequently, the function $F(\phi, \theta)$ are real. In this way, the lower bound inequality in (9) can be rewritten as a convex constraint. In fact, since the real function $F(\phi, \theta)$ is close to its maximum value in the bounded area $C$, it is plausible that within $C$ it is also strictly positive; thus, the inequality can be simplified as $F(\phi_k, \theta_k) \geq 10^{P_{\text{bound}}/20}$, $(\phi_k, \theta_k) \in C$, and, finally, written in the form $-F(\phi_k, \theta_k) \leq 10^{P_{\text{bound}}/20}$, $(\phi_k, \theta_k) \in C$ that can be included as a convex constraint in the optimization.

The optimization problem (9) for the broadside direction can now be written as

$$
\begin{aligned}
\min_{w_n, \, n \in \{1, \ldots, N\}} \quad & t \\
\text{s.t.} \quad & F(\phi_0, \theta_0) = 1 \\
& |F(\phi_i, \theta_i)| \leq t, \, (\phi_i, \theta_i) \in \Sigma \\
& F(\phi_j, \theta_j) = 10^{\frac{P_{\text{bound}}}{20}}, \, (\phi_j, \theta_j) \in B \\
& |F(\phi_h, \theta_h)| \leq 10^{\frac{P_{\text{bound}}}{20}}, \, (\phi_h, \theta_h) \in \Omega \\
& F(\phi_k, \theta_k) \leq 1, \, (\phi_k, \theta_k) \in C \\
& -F(\phi_k, \theta_k) \leq -10^{\frac{P_{\text{bound}}}{20}}, \, (\phi_k, \theta_k) \in C
\end{aligned}
\tag{11}
$$

The last constraint has been introduced because in the case of a high number of antennas, the array factor exhibits very large oscillations which might cause the function $F(\phi, \theta)$ to be lower than $10^{P_{\text{bound}}/20}$ within the coverage area.

The optimization problem in (11) can now be written in the form of a linear program as described in [15] with the great advantage of a lower computational complexity.

### 3.1.2 Non-broadside array

When the mechanical tilt $\theta_A$ cannot be arbitrarily steered to comply with a specific coverage direction, or if it is necessary to synthesize more coverage areas toward different directions, the synthesis function in (4) is not real because $w_n \in \mathbb{C}$, $n \in \{1, .., N\}$. For this reason, another simplification of the problem is herein

proposed. In fact, if a particular shape of the weights is chosen, that is, $w_n = a_n e^{-j(k_{x,0}x_n + k_{y,0}y_n)}$, where $a_n \in \mathbb{R}$, $n \in \{1, .., N\}$, $k_{x,0} = k_x(\phi = \phi_0, \theta = \theta_0)$, and $k_{y,0} = k_y(\phi = \phi_0, \theta = \theta_0)$, the synthesis function (4) reads

$$F(\phi, \theta) = 2\frac{r_0}{r}\frac{f(\phi, \theta)}{f(\phi_0, \theta_0)} \cdot \sum_{n=1}^{\frac{N}{2}} a_n \cos\left[(k_x - k_{x,0})x_n + (k_y - k_{y,0})y_n\right] \qquad (12)$$

which is again a real function. As for the broadside array case, the optimization problem (9) in the known direction $(\phi_0, \theta_0)$ can be simplified as (11) and written in the form of a linear program as described in [15].

### 3.2 Simulation results

In this section, some numerical results which demonstrate the capability of the described method are presented. A circular shape for both the coverage area and the suppression region is considered, with diameter of 3.5 and 6.5 m, respectively. The two regions are centered in $(0, y_0)$ and $h_A = 5.5$ m. A rectangular array of $N_x \times N_y$ elements with uniform interelement distance $d = 0.6\lambda_0$ is synthesized, with antenna elements as microstrip patch antennas (theoretical formula of the radiation pattern $f(\phi, \theta)$ has been taken as reported in [2, 19]).

The linear problem has been solved by the function **linprog** of the commercial software MATLAB [20]. The optimization has been done with a resolution of 0.25 m on the coverage area plane, with a total of 120,000 points. Both the coverage area and suppression region boundaries have been discretized with four points.

The antenna array normalized electric field when $\theta_A = 60°$, $y_0 = 3.25$ m, and $P_{\text{bound}} = -10$ dB is shown in **Figure 5(a)**, achieved with the broadside optimization and an array of size $16 \times 12$. **Figure 5(b)** also depicts the contour plot of the synthesized normalized electric field.

Good agreement between the required coverage area and the synthesized one confirms the capability of the proposed method. Furthermore, this result has been obtained in less than 2 minutes with a 2.6 GHz Intel Core i7 processor, which is important to prove the good trade-off between performance and computational complexity are achieved by the described solution.
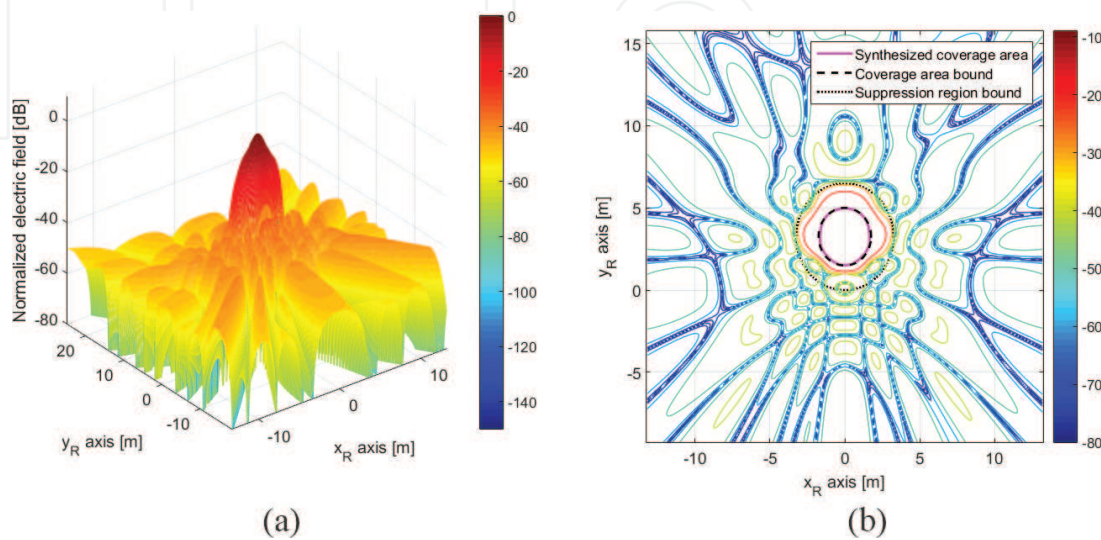


**Figure 5.**
*Antenna array normalized electric field with an array of size 16 × 12 when $\theta_A = 60°$, $y_0 = 3.25$ m, $P_{\text{bound}} = -10$ dB, and broadside optimization. (a) Normalized electric field in $x_R$ and $y_R$ axes and (b) normalized electric field contour plot.*
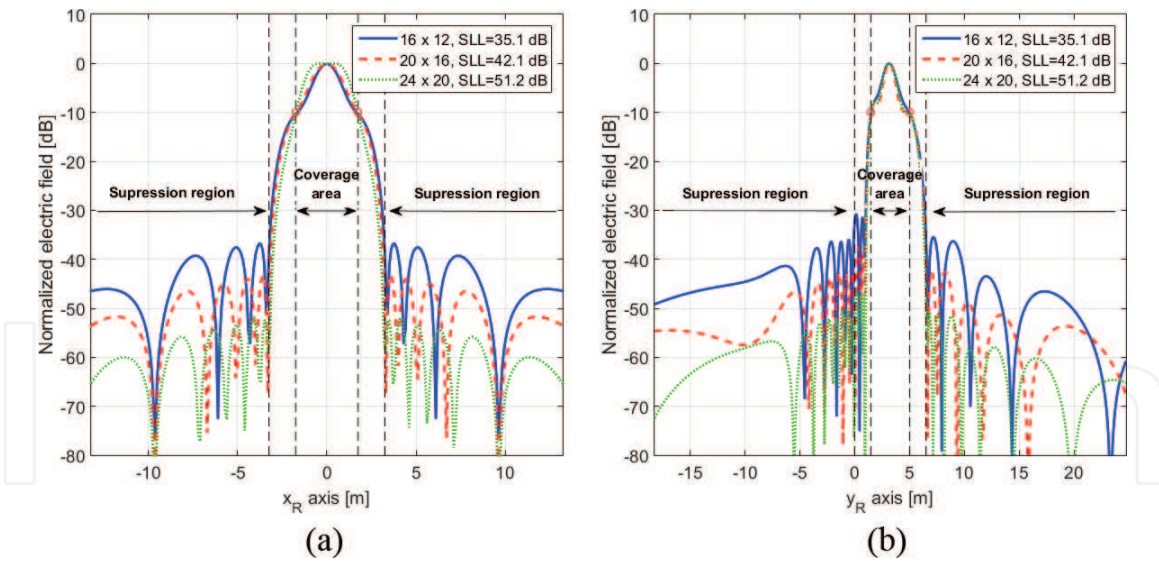
**Figure 6.**
*Antenna array normalized electric field with different numbers of antenna elements, with $\theta_A = 60°$,*
*$y_0 = 3.25\ m$, $P_{bound} = -10\ dB$, and broadside optimization. (a) Normalized electric field in $x_R$ axis, within*
*$y_R = 3.25\ m$, and (b) normalized electric field in $y_R$ axis, within $x_R = 0\ m$.*

Now, the effectiveness of the proposed method is investigated for different synthesis parameters.

The broadside optimization presented in Section 3.1.1 is firstly analyzed for different numbers of antenna elements. Results are reported in **Figure 6** as a function of the coordinates $x_R$ and $y_R$, with $\theta_A = 60°$, $y_0 = 3.25$ m, and $P_{bound} = -10$ dB.

The curve $16 \times 12$ is the first feasible result which presents a sidelobe level of 35.1 dB within the suppression region. Other curves have been obtained with increased number of antenna elements. Obviously, the sidelobe-level performance improves with the increase of the antenna elements. All the synthesized results respect the $P_{bound}$ constraint.

The influence of the mechanical tilt $\theta_A$ choice on the optimization result is herein investigated. Broadside optimization along with the coordinate $y_R$ for different mechanical tilt $\theta_A$ is depicted in **Figure 7(a)**. It is worth noting that the coverage
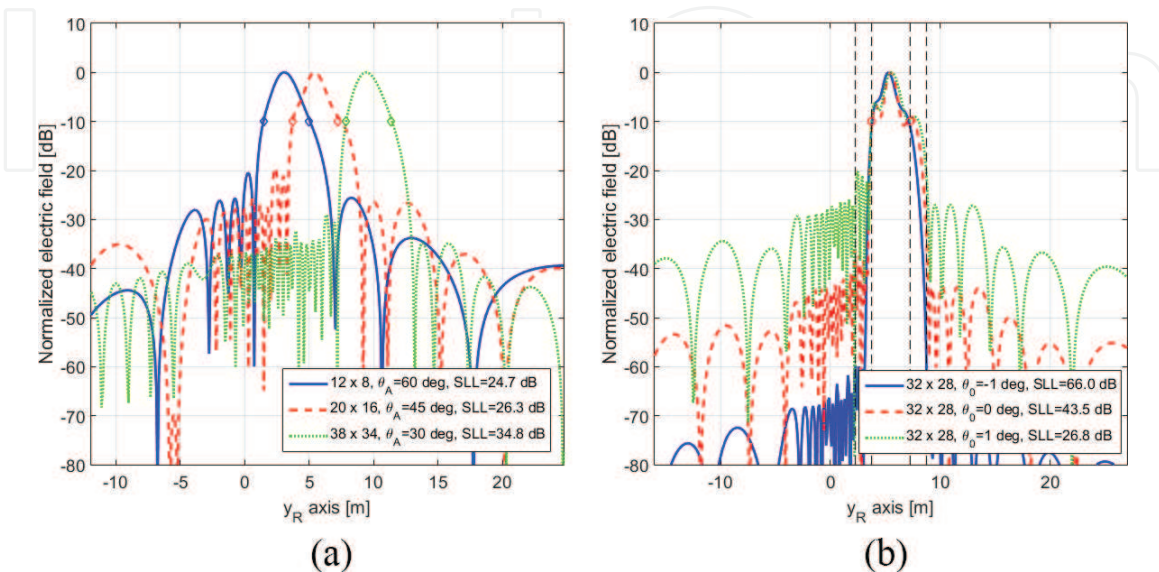


**Figure 7.**
*(a) Antenna array normalized electric field with different mechanical tilt $\theta_A$ in $x_R = 0\ m$, with*
*$P_{bound} = -10\ dB$, and broadside optimization and (b) antenna array normalized electric field with different*
*steering directions $\theta_0$ in $x_0 = 0\ m$, with $y_0 = 3.25\ m$, and $P_{bound} = -10\ dB$.*

area center position $y_0$ has been progressively increased to be the points on the coverage area plane which corresponds to the broadside direction, that is, $y_0 = 3.25$ m with $\theta_A = 60°$, $y_0 = 5.5$ m with $\theta_A = 45°$, and $y_0 = 9.5$ m with $\theta_A = 30°$, and that the array is assumed to be of minimum size.

It is of interest to observe that a decrease in mechanical tilt leads to a decrease in the required beamwidth and, consequently, an increase in the required array size. The achieved sidelobe levels are larger than 20 dB.

The non-broadside case is also considered. In **Figure 7(b)** the performance of the broadside optimization and the non-broadside optimization is compared in order to confirm the steering direction choice discussed in Section 3.1.

It is clear from **Figure 7(b)** that the choice of the steering direction affects the sidelobe level outside the coverage area. In fact, a 1° decrease in the steering direction with respect to the broadside, that is, the steering direction which corresponds to the coverage area center point, yields a sidelobe-level improvement of 22.5 dB. On the other hand, an increase of 1° leads to a sidelobe deterioration.

## 4. Coverage area synthesis for RFID-based ETC system

After the description of a general optimization procedure for a pattern defined on a planar surface (which can be used for the synthesis of a high data-rate service area), in this section we will consider the coverage area synthesis problem from the ETC application point of view. As briefly described in Section 1, the objective of a coverage area synthesis in this context should be the maximization of the communication area length in the travel direction and not the synthesis of a specific pattern geometry. For this case, an optimization procedure similar to the one described in Section 3 might also be derived. Nonetheless, channel phenomena, for example, fading [21], are known and, together with other possible implementation tolerances, might lead to suboptimal solutions in spite of the synthesis effort.

For this reason, a simple iterative methodology for synthesizing a planar antenna array with both the aim of stretching the coverage area toward the longitudinal direction and confining it within a roadlane is described. This method has the advantage of providing acceptable results with a reduced number of antenna elements with respect to the optimization presented in Section 3.

### 4.1 RFID-based DSRC system

RFID technology is usually employed for the implementation of DSRC because of its well-known advantages of excellent accuracy and the possibility to be read at high speed [22]. A RFID-based DSRC system is basically realized by means of a RSU beacon reader, raised installed in order to guarantee sufficient visibility, and some OBU transponders. Moreover, antennas are constrained to radiate with circular polarization (CP) for two main reasons: CP reduces polarization mismatch due to reciprocal rotation between RSU and OBU devices and improves immunity to multipath effect [23]. The latter is a fundamental characteristic which guarantees the validity of a free space propagation loss model [21].

The coverage area definition is based on the threshold power $P_{bound}$ which, in the case of a monostatic backscatter [22] RFID-based system, can be interpreted as the tag sensitivity threshold $P_{tag, th}$ and the reader sensitivity $P_{reader, th}$. Therefore,

according to the free space propagation model, the communication area is defined as the set of coordinates $x_R$ and $y_R$ in the reference plane $z_R = h_{tag}$ in which

$$
\begin{cases}
P_{\text{forward}}(x_R, y_R) = P_t + G_t(\phi, \theta) + G_r + 20 \log_{10}\left(\frac{\lambda_0}{4\pi r}\right) \geq P_{\text{tag, th}} \\
P_{\text{back}}(x_R, y_R) = P_{\text{forward}}(x_R, y_R) + G_t(\phi, \theta) + G_r + 20 \log_{10}\left(\frac{\lambda_0}{4\pi r}\right) + 10 \log_{10}M \geq P_{\text{reader, th}}
\end{cases}
$$

(13)

where $P_t$ is the transmitted power, $G_t(\phi, \theta) = G_{t,\,\max} + 20 \log_{10}F(\phi, \theta)$ represents the antenna array gain pattern (which includes the normalized synthesis function), $G_r$ is the tag gain, and $M$ is the modulation factor (for a passive tag, $M = 0.25$ [22]).

**4.2 Antenna array synthesis with iterative method**

Let us consider the normalized synthesis function in (6) for a rectangular planar array of $N_x \times N_y$ elements with uniform interelement distances $d_x$ and $d_y$ which can be rewritten as

$$
F(\phi, \theta) = \frac{r_0}{r} \frac{f(\phi, \theta)}{f(\phi_0, \theta_0)} \sum_{n=1}^{N_x} \sum_{m=1}^{N_y} w_{n, m} e^{j\left[k_x(n-1)d_x + k_y(m-1)d_y\right]}
$$

(14)

The synthesis problem is basically the definition of:

- Number of antenna elements $N_x$ and $N_y$

- Interelement distances $d_x$ and $d_y$

- Complex excitations $w_{n, m}$

A simple iterative method to synthesize the coverage area with the objective of stretching its length toward the travel direction is described [16]. In this case, complex coefficients $w_{n, m}$ are taken as in (12), that is, $w_{n, m} = a_{n, m} e^{j\left[(k_x - k_{x, 0})(n-1)d_x + (k_y - k_{y, 0})(m-1)d_y\right]}$, with $a_{n, m}$ based on Tschebyscheff coefficients and $R_x$ and $R_y$ the Tschebyscheff design sidelobe level [2].

Then, the synthesis process can be performed according to the following steps:

1. Initialize the steering direction toward broadside ($\phi_0 = 0, \theta_0 = 0$), $R_x = R_y = 10$ dB, and the parameters $d_x$ and $d_y$ according to the antenna design requirements, for example, directivity, mutual coupling, size constraints, etc.

2. Starting from a minimum size $N_x = 2$ and $N_y = 2$, increase the antenna array dimension $N_y$ to cover a little bit more than the required transverse width.

3. Adjust the sidelobe level $R_y$ according to the required horizontal power margin requirements.

4. Increase the antenna array dimension $N_x$ in accordance with the antenna gain requirements.

5. Adjust the sidelobe level $R_x$ to obtain the required vertical power margin.

6. Choose the best steering elevation $\theta_0$ in the sense of maximizing the length of the coverage area along with the coordinate $y_R$ (with starting coordinate $y_R = 0$).

Each step is iteratively executed to compare the Tschebyscheff synthesis results and verify the conditions in (13) and then determine the coefficients $a_{n,m}$.

### 4.3 Synthesis example and experimental results

A coverage area synthesis is herein described for the case of a reader height $h_A = 5.5$ m with mechanical tilt $\theta_A = 45°$. and OBU height $h_{tag} = 1.5$ m. System parameters are chosen according to the standard EPC Gen2 for UHF RFID [24] for the carrier frequency 920 MHz which limits the *effective isotropic radiated power* to the value $P_{EIRP} = P_t + G_{t,\,max} = 36$ dBm. After that, the other parameters are $G_r = 5$ dBi, $P_{tag,\,th} = -20$ dBm (the sensitivity of the commercial product Impinj Monza R6 [25]), and $P_{reader,\,tag} = -84$ dBm (the sensitivity of the commercial product Impinj Indy R2000 [26]).

Following the synthesis process described above, the optimized coverage area for a 6 m road width is achieved as depicted in **Figure 8(a)**, with the following synthesis parameters: $N_x = 4$, $N_y = 4$, $d_x = 0.45\lambda_0$, $d_y = 0.48\lambda_0$ (with $\lambda_0$ evaluated at 920 MHz), $\theta_0 = -5°$, $R_x = 30$ dB, $R_y = 25$ dB, and the coefficients as in [27].

The achieved coverage area is 8 m long, covers the required transversal direction width, and presents very low lateral sidelobes. **Figure 8(b)** also presents the achieved coverage area at $h_{tag} = 2.5$ m (it could represent the tag height of a truck) and $h_{tag} = 1$ m (that can represent the tag height of a motorcycle) along with the coordinate $y_R$, and it shows that the higher the tag height $h_{tag}$, the shorter the coverage area. This is acceptable because the speed of a truck is usually lower than the speed of a common vehicle, so the available transaction time will be longer.

In order to confirm the simulation results, the synthesized antenna array has been designed and manufactured, as shown in **Figure 9(a)**. The design process of the $4 \times 4$ CP microstrip patch antenna array is described in [27]. Furthermore, the 12 dBi RHCP gain antenna prototype has been fixed at the height $h_A = 5.5$ m with a metallic scaffolding and used for collecting experimental results, as depicted in **Figure 9(b)**. A commercial Impinj Speedway R420 UHF reader [28] ($P_{reader,\,th} = -84$ dBm) and a tag device with $P_{tag,\,th} = -32$ dBm have been
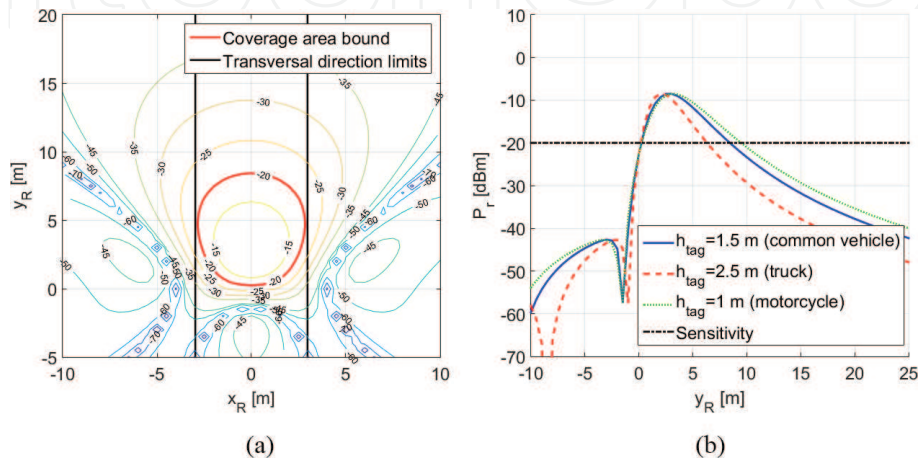


(a)                    (b)

**Figure 8.**
*Synthesis example of the coverage area at 920 MHz. (a) Received power contour plot at $h_{tag} = 1.5$ m and (b) received power profile along $y_R$ coordinate as function of the tag height $h_{tag}$.*
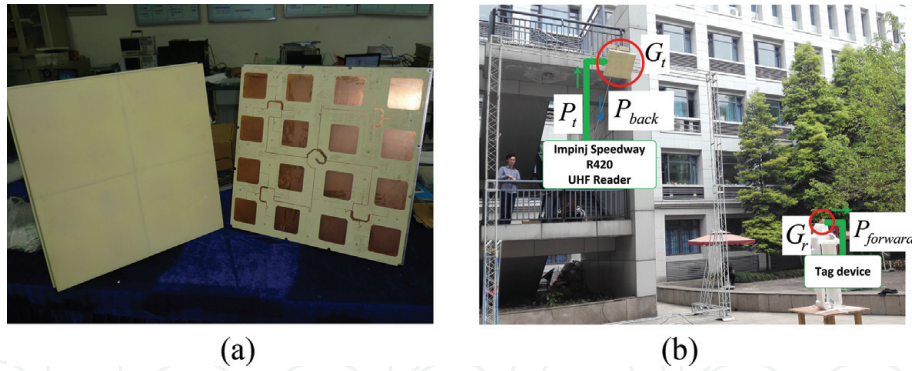
**Figure 9.**
*(a) 4 x 4 CP microstrip patch antenna array fabricated prototype and (b) experimental setup for the ETC antenna array system measurement.*

employed. A compact CP UHF antenna with gain $G_r = 4$ dBi has been used as tag antenna.

The transmitted power $P_t$ has been regulated in the range $5 \div 30$ dBm for each position of the tag device in the road plane $(x_R, y_R)$ to determine the minimum value $P_{t,min}$ which activates the tag, that is, $P_{forward}(x_R, y_R) = P_{t,\min} + G_t(\phi, \theta) + G_r + 20 \log_{10}\left(\frac{\lambda_0}{4\pi r}\right) = P_{tag,th}$, under the condition that $P_{back}(x_R, y_R) \geq P_{reader,th}$. After that, in a similar way to what has been described in [29], the power $P_{forward}(x_R, y_R)$ when a limited $P_{EIRP} = 36$ dBm is applied and a specific $P_{tag,th} = -20$ dBm is chosen has been inferred as $P_{forward}(x_R, y_R) = P_{tag,th} + P_{EIRP} - P_{t,min} - G_{t,max}$ (cable losses have been compensated during the power evaluation). Experimental results are shown in **Figure 10(a)** and **(b)**.

Good correspondence among simulations (SR), antenna measurement projection on the road plane (AM), and experimental results (ER) is visible, and only few discrepancies arise. These are mainly due to the 1 dB tag antenna gain reduction with respect to the design parameter, the tag antenna radiation pattern (not taken into account), and other possible errors in fixing the antenna mechanical tilt $\theta_A$.
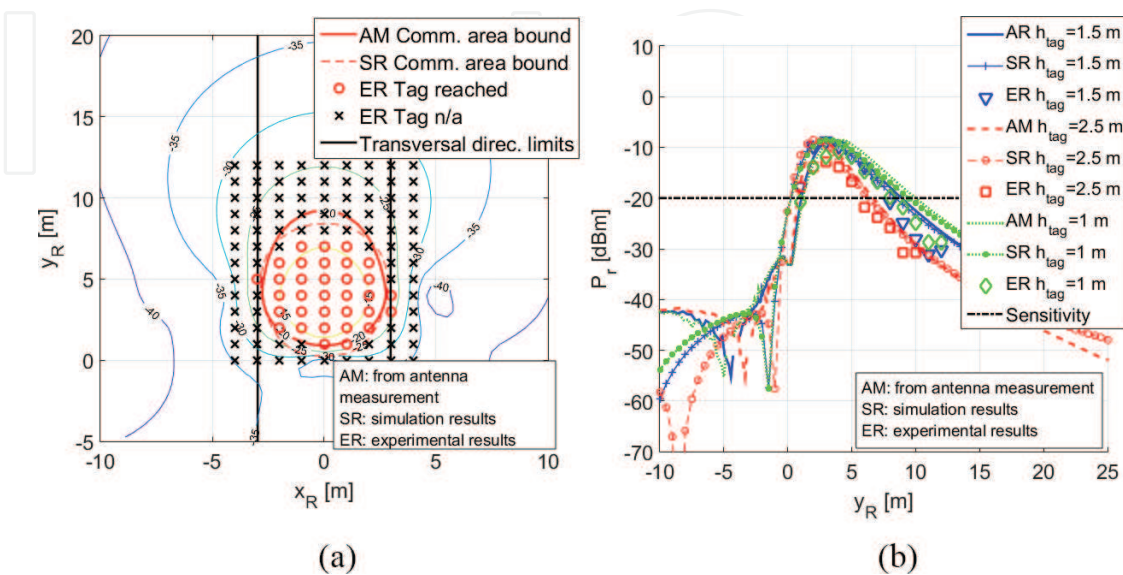


**Figure 10.**
*Comparison of synthesis results obtained by projecting the measurement results of the antenna to the road plane (AM), simulation (SR), and experimental results (ER). (a) Received power contour plot at $h_{tag} = 1.5$ m and (b) received power profile along $y_R$ coordinate as function of $h_{tag}$.*

## 5. Conclusions

The optimization of an antenna array pattern when the electric field $r$-decay factor effect cannot be neglected has been described, with particular emphasis on the context of DSRC systems. In fact, in order to maximize the available transaction time of ETC for future MLFF, it has been shown that particular attention has to be dedicated to the antenna array beam pattern synthesis on the road surface (or in a parallel surface plane). The generic optimization problem of a beam pattern defined on a planar surface has been introduced with the concept of coverage area. The coverage area is a bounded portion of the space in which the communication between RSU and OBU has to be guaranteed. After that, an optimization algorithm for specific coverage area geometries has been derived and solved through linear programming, highlighting the difficulties in achieving the synthesis due to the $r$-decay factor effect. Then, the design of the antenna array for maximizing the coverage area length in the specific RFID-based ETC case by employing a simple iterative method has been described. A $4 \times 4$ planar antenna array for UHF EPC Gen2 standard has been manufactured and employed as reader antenna during a measurement procedure which has demonstrated the validity of the proposed methodology.

## Acknowledgements

## Conflict of interest

The authors declare that there is no conflict of interests regarding the publication of this chapter.

## Author details

Daniele Inserra* and Guangjun Wen
School of Information and Communication Engineering, University of Electronic Science and Technology of China, Chengdu, China

*Address all correspondence to: inserradaniele@uestc.edu.cn

IntechOpen

## References

[1] Kummer WH. Basic array theory. Proceedings of IEEE. 1992;**80**(1): 127-140. DOI: 10.1109/5.119572

[2] Balanis CA. Antenna Theory: Analysis and Design. 3rd ed. Hoboken: John Wiley & Sons, Inc.; 2005. 1117 p

[3] Bevelacqua PJ, Balanis CA. Minimum sidelobe level for linear array. IEEE Transactions on Antennas and Propagation. 2007;**55**(12):3442-3449. DOI: 10.1109/TAP.2007.910490

[4] Fuchs B. Shaped beam synthesis of arbitrary arrays via linear programming. IEEE Antennas Wireless Propagation Letters. 2010;**9**:481-484. DOI: 10.1109/LAWP.2010.2051210

[5] Lebret H, Boyd S. Antenna array pattern synthesis via convex optimization. IEEE Transactions on Signal Processing. 1997;**45**(3):526-532. DOI: 10.1109/78.558465

[6] Marcano D, Duran F. Synthesis of antenna arrays using genetic algorithms. IEEE Antennas Propagation Magazine. 2000;**42**(3):12-20. DOI: 10.1109/74.848944

[7] Bevelacqua PJ, Balanis CA. Optimizing antenna array geometry for interference suppression. IEEE Transactions on Antennas and Propagation. 2007;**55**(3):637-641. DOI: 10.1109/TAP.2007.891509

[8] Semenov B. Effective iterative methods for contoured beams reflector antenna synthesis. In: Proceeding of the IEEE 39th European Microwave Conference (EuMC 2009); 29 September-1 October. Vol. 2009. Rome, Italy: IEEE; 2009. pp. 1500-1503. DOI: 10.23919/EUMC.2009.5296389

[9] Chou HT, Hsiao YT, Pathak P, Nepa P, Janpugdee P. A fast DFT planar array synthesis tool for generating contoured beams. IEEE Antennas Wireless Propagation Letters. 2004;**3**: 287-290. DOI: 10.1109/LAWP.2004.837504

[10] Chou HT. An efficient successive projection method for the synthesis of phased array antennas to radiate contoured field patterns. In: Proceedings of IEEE International Conference on Wireless Information Technology and Systems (ICWITS 2012); 11–16 November 2012; Maui, HI. USA: IEEE; 2012. pp. 1-4. DOI: 10.1109/ICWITS.2012.6417699

[11] Poulton GT. Power pattern synthesis using the method of successive projections. In: Proceeding of IEEE Antennas and Propagation Society International Symposium (AP-S); 8–13 June 1986; Philadelphia. PA, USA: IEEE; 1986. pp. 667-670. DOI: 10.1109/APS.1986.1149679

[12] Han Y, Wan C, Sheng W, Tian B, Yang H. Array synthesis using weighted alternating projection and proximal splitting. IEEE Antennas Wireless Propagation Letters. 2015;**14**:1005-1009. DOI: 10.1109/LAWP.2015.2389804

[13] Shieh WY, Lee WH, Tung SL, Ho CD. A novel architecture for multilane-free-flow electronic-toll-collection systems in the millimeter-wave range. IEEE Transactions on Intelligent Transportation Systems. 2005;**6**(6): 294-301. DOI: 10.1109/TITS.2005.853708

[14] Inserra D, Wen G. Communication area synthesis for next generation highway ETC systems. In: Proceeding of IEEE International Conference on Communications in China (ICCC '16); 27–29 July 2016; Chengdu. China: IEEE; 2016. pp. 1-6. DOI: 10.1109/ICCChina.2016.7636820

[15] Inserra D, Wen G, Hu W. Linear optimization of antenna array for radiation pattern defined on a planar surface. Journal of Electromagnetic Waves and Applications. 2018. DOI: 10.1080/09205071.2018.1488624

[16] Inserra D, Hu W, Wen G. Antenna array synthesis for RFID-based electronic toll collection. IEEE Transactions on Antennas and Propagation. 2018. DOI: 10.1109/TAP.2018.2851292

[17] Inserra D, Wen G, Hu W. Planar antenna array design considerations for RFID electronic toll collection systems. In: Proceeding of IEEE MTT-S International Wireless Symposium (IWS '16); 14–15 March 2016; Shanghai. China: IEEE; 2016. pp. 1-4. DOI: 10.1109/IEEE-IWS.2016.7585452

[18] Bevelacqua P. Antenna arrays: Performance limits and geometry optimization [Ph.D thesis]. Arizona State University; 2008

[19] Carver K, Mink J. Microstrip antenna technology. IEEE Transactions on Antennas and Propagation. 1981; **29**(1):2-24. DOI: 10.1109/TAP.1981.1142523

[20] MATLAB, version 7.10.0 (R2010a). Natick, Massachusetts: The MathWorks Inc.; 2010

[21] Rappaport TS. Wireless Communications: Principles and Practice. United States: Prentice Hall; 1996

[22] Finkenzeller K. RFID Handbook. 3rd ed. Chichester: Wiley; 2010. 462 p

[23] Cidronali A, Maddio S, Passafiume M, Manes G. Car talk: Technologies for vehicle-to-roadside communications. IEEE Microwave Magazine. 2016;**17**(11): 40-60. DOI: 10.1109/MMM.2016.2600949

[24] EPCglobal Std. EPC Radio Frequency Identify Protocols Class-1 Generation-2 UHF RFID, Protocol for Communications at 860–960 MHz. Rev. version 1.1.0. 2005

[25] Impinj Monza R6-P tag chip datasheet. [Internet]. Available from: https://wwww.impinj.com/platform/endpoints/monza-r6/

[26] Impinj Indy R2000 UHF Gen2 RFID reader chip datasheet. [Internet]. Available from: https://www.impinj.com/platform/connectivity/indy-r2000/

[27] Inserra D, Hu W, Wen G. Design of a microstrip series power divider for sequentially rotated non uniform antenna array. International Journal of Antennas and Propagation. 2017. DOI: 9482979. 8 p. DOI: 10.1155/2017.9482979

[28] Impinj Speedway R420 RFID reader datasheet. [Internet]. Available from: https://www.impinj.com/platform/connectivity/speedway-r420/

[29] Colella R, Catarinucci L, Coppola P, Tarricone L. Measurement platform for electromagnetic characterization and performance evaluation of UHF RFID tags. IEEE Transactions on Instrumentations and Measurement. 2016;**65**(4):905-914. DOI: 10.1109/TIM.2016.2516322